Complex balancing motions of an inverted pendulum subject to delayed feedback control

J. Sieber and B. Krauskopf

Bristol Centre for Applied Nonlinear Mathematics, Department of Engineering Mathematics, Queen's Building, University of Bristol, BS8 1TR, U.K.

Abstract

We show that an inverted pendulum that is balanced on a cart by linear state-dependent delayed control may exhibit small chaotic motion about the upside-down position. In periodic windows associated with this chaotic regime we find periodic orbits of arbitrarily high period that correspond to complex balancing motion of the pendulum with bounded velocity of the cart.

This result shows that complex balancing is possible in a controlled mechanical system with a geometric nonlinearity even when the control law is only *linear*. This is in contrast to other proposed models that require a nonlinearity of the controller, such as round-off due to digitization.

We find the complex motion by studying homoclinic bifurcations of a reduced three-dimensional vector field near a triple-zero eigenvalue singularity. More generally, the dynamics we describe must be expected in any system with a triple-zero singularity and reflection symmetry.

Key words: inverted pendulum, balancing motion, feedback control, delay differential equation, triple-zero singularity, homoclinic tangency
PACS: 05.45, 02.30.Ks

1 Introduction

Balancing a long stick is easier than balancing a short stick. This well-known fact is due to the human reaction time, which introduces the effect of a time delay into this control problem. This reaction time is about 100 ms for eye-hand coordination [1], which is not negligible for a short stick (about 30 cm) since the inherent time scale for the stick motion is of the same order [2]. In fact, any stabilization scheme using state-dependent feedback control will be adversely affected by control loop latency, that is, a non-zero reaction time between the measurement of the state of the system and the control action.

Delay-induced instabilities have been studied extensively in other systems with delay, for example, in coupled neurons [3,4], lasers subject to optical feedback due to external reflections [5], and in cutting processes [6].

We consider here the idealized model of balancing control, namely an inverted planar pendulum on a moving cart that is stabilized by a state-dependent control force D; see Fig. 1 and Sec. 2 for the mathematical details. Due to the latency of the control loop, the control force takes effect only after some fixed delay τ. This leads to a mathematical description by a delay differential equation (DDE) with an infinite-dimensional phase space; see [7,8] as general references to the theory of DDEs. The DDE is symmetric with respect to reflection at the origin, the upside-down position of the pendulum, due to the reflection symmetry of the pendulum. Perfect control is achieved when the upside-down position is stable, while the cart moves with constant velocity. (This velocity at the stable limit can be brought to zero by choosing a suitable initial condition or by introducing a small amount of damping.)

Linear stability analysis shows that there is a region in the parameter space of the controller where perfect control can be achieved, provided the delay τ is not too large [2,9]. Furthermore, stability is generally lost in a Hopf bifurcation. It is possible to compute the criticality of this Hopf bifurcation, which gives a first idea of how the system behaves beyond the stability boundary [9–11]. If the Hopf bifurcation is supercritical then the pendulum performs (initially) small oscillations about the upside-down position but with finite velocity of the cart. Such small oscillations have been observed in experiments [11]. They are an example of a relaxed form of stabilization that we call *balancing motion* (much like what actually happens when you balance a stick). Such a balancing motion is stable and bounded around the upside-down position while the velocity of the cart is also bounded.

It has been an open question whether there are more complex balancing motions in the system apart from perfect stabilization and simple oscillations after the first Hopf bifurcation. Mathematically, such balancing motion corresponds to a symmetric attractor of the system with bounded velocity of the cart. It is not straightforward to find complex balancing motions of the inverted pendulum. Indeed, bifurcation analysis shows that any such solution in the controlled pendulum, if it exists, cannot be found by simply following the bifurcations of the initial symmetric periodic orbits [13]. In particular, the simple oscillations lose their stability in a symmetry breaking bifurcation (pitchfork bifurcation of periodic orbits), which results in a complete loss of control [9,13]. There are now two (symmetrically related) periodic orbits. Each of these nonsymmetric periodic orbits corresponds to the pendulum wanting to fall to one side, which the controller will attempt to compensate for by increasing the velocity of the cart. Hence, the parameter region where nonsymmetric regimes are prevalent is typically not regarded as physically relevant.

Computer-based balancing experiments have shown chaotic balancing motions with small amplitudes, referred to as micro chaos [12]. However, this dynamics is due to discontinuities associated with digital sampling in time and space. Consequently, the results in Ref. [12] leave the general question open whether complex nonlinear vibrations are possible entirely within the setting of *linear control* of a mechanical system with a geometric nonlinearity.

In this paper we show that complex balancing motions of the linearly controlled inverted pendulum exist, which answers this general question to the positive. Specifically, we find bounded symmetric chaotic motion of the pendulum around its upside-down position inside the parameter region associated with pairs of nonsymmetric attractors. This motion consists of long stretches where the pendulum is about to fall over to one side and the cart speeds up to compensate, followed by another stretch where the pendulum is about to fall over to the other side and the cart reverses direction. The velocity of the cart performs a chaotic motion as well with long, irregular excursions in the positive and negative directions that may leave any bounded region. This chaotic motion is not balancing according to our definition requiring bounded velocity of the cart, but associated with it there are stable symmetric periodic orbits of arbitrarily large period. Since they have bounded velocity of the cart, these periodic orbits correspond to complex balancing motion. The parameter islands where these balancing motions occur, so-called periodic windows in the parameter space, are not connected to the primary family of symmetric periodic orbits that emerged from the Hopf bifurcation.

We obtain these results by considering a three-dimensional vector field, derived first in Ref. [13] (see Section 2.1), describing the dynamics on the center manifold reduction of the system near a codimension-three triple-zero eigenvalue bifurcation. Reference [13] considers only the bifurcation diagram related to the loss of stability of the origin, the perfectly balanced upside-down position of the pendulum, and the onset of small stable oscillations. In this paper we consider the parameter region where the primary oscillations are of saddle type. After the reduction to a (symmetric) local Poincaré map, this oscillation corresponds to a symmetric saddle fixed point with one-dimensional stable and unstable manifolds. Well established numerical algorithms [14] allow us to locate a first quadratic tangency of these manifolds. Then, the existence of infinitely many stable symmetric periodic orbits of arbitrarily large period follows from general statements on homoclinic tangencies [15] in two-dimensional maps. Furthermore, the pair of nonsymmetric attractors merge and form a single symmetric chaotic attractor in a crisis bifurcation [16]. These theoretical results are indeed of relevance for the original control system, which is demonstrated by showing examples of merging chaotic attractors and symmetric periodic orbits of long period in the full DDE.

The mechanism we describe in this paper is not specific to our particular

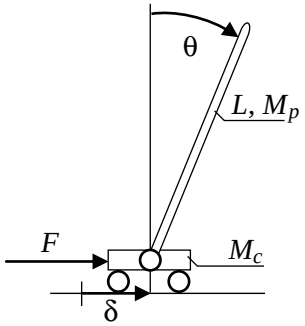

Fig. 1. Sketch of the inverted pendulum of length L and mass M_p on a cart of mass M_c at horizontal position δ. The inclination angle θ is defined such that it is positive in the position shown in the sketch.

model system, but is directly associated with the symmetric triple-zero singularity. One must expect crisis bifurcations and complicated symmetric attractors in any system that features this singularity. Interestingly, the triple-zero singularity appears to be prevalent when a control loop controlling a saddle equilibrium is subject to delay. For example, Ref. [17] investigated the inverted pendulum subject to a PMD (proportional minus delay) controller and found the same singularity when increasing the control loop latency; see [18] for other examples.

The paper is organized as follows. We first introduce the details of the mathematical model in Sec. 2, where we also explain the center manifold reduction and present the bifurcation diagram of the reduced three-dimensional vector field model near the triple-zero eigenvalue bifurcation. In Sec. 3 we show that there are complex symmetric dynamics in the reduced model, and in Sec. 4 we give examples of complex balancing motion in the full control system. Finally, in Sec. 5 we conclude and point to some open problems.

2 Model equations

The dynamics of the setup in Fig. 1 are governed by the second-order differential equation for the angular displacement θ of the pendulum, which can be written as (see also Refs. [2,9,17]):

$$\left(1-\frac{3m}{4}\cos^2\theta\right)\ddot{\theta}+\frac{3m}{8}\dot{\theta}^2\sin(2\theta)-\frac{3}{2}\frac{g}{L}\sin\theta+\frac{3F}{2L(M_p+M_c)}\cos\theta=0. \quad (1)$$

Here, F is the horizontal driving force applied to the cart, and $m=M_p/(M_p+M_c)$ is the ratio of the mass of the uniform pendulum M_p with respect to the sum of the mass of the cart M_c and the mass of the pendulum. The length of the pendulum is L and g is the gravitational acceleration. We adjust the time

scale to the intrinsic time scale of the pendulum by rescaling time introducing a new dimensionless time $t_{\text{new}} = t_{\text{old}} \cdot \sqrt{3g}/\sqrt{2L}$. This converts equation (1) to its dimensionless form

$$\left(1 - \frac{3m}{4}\cos^2\theta\right)\ddot{\theta} + \frac{3m}{8}\dot{\theta}^2\sin(2\theta) - \sin\theta + D\cos\theta = 0 \tag{2}$$

where $D = F/(g(M_c + M_p))$ is the rescaled horizontal driving force. Because friction is not taken into account, the equation of motion for the displacement δ of the cart does not couple back into (2). It reads

$$\ddot{\delta}(t) = L\frac{\frac{m}{2}\sin\theta\dot{\theta}^2 + \frac{2}{3}D - \frac{m}{4}\sin(2\theta)}{1 - \frac{3m}{4}\cos^2\theta} \tag{3}$$

when also written with respect to the dimensionless time. The force D is applied as a feedback control depending on the state of the system with the goal of stabilizing the pendulum at its upright position, which is $\theta = 0$. The feedback control force D is a function of the state of the system at some fixed time τ ago, where τ is the latency of the overall system. We study the case of a linear PD (proportional plus derivative) control force

$$D(t) = a\theta(t - \tau) + b\dot{\theta}(t - \tau) \tag{4}$$

which is given by the control gains a and b. It features a single fixed delay time $\tau > 0$ in the controller and converts the differential equation (2) into a DDE. This delay τ in the dimensionless time corresponds to a delay of $\tau \cdot \sqrt{2L}/\sqrt{3g}$ in the original time.

2.1 Center manifold reduction

We now show how one can reduce the DDE (2) to a system of ordinary differential equations (ODEs) on a three-dimensional local center manifold around the origin. This follows the procedure as outlined, for example, in Refs. [7,8]. The material presented here allows the reader to link back the results of section 3 to the original DDE (2). After rescaling time back by $\sqrt{2L}/\sqrt{3g}$, the results can be interpreted in terms of the original physical quantities in (1).

First, we rescale time and angular velocity such that the delay is 1, and equation (2) is a DDE of the form

$$\dot{x}(t) = f(x(t), x(t-1), \lambda) \tag{5}$$

where the right-hand-side $f : \mathbb{R}^2 \times \mathbb{R}^2 \times \mathbb{R}^4 \to \mathbb{R}^2$ is

$$\begin{aligned} f_1(x, y, \lambda) &= x_2 \\ f_2(x, y, \lambda) &= \frac{-\frac{3}{8}m \sin(2x_1)x_2^2 + \tau^2 \sin x_1 - \cos x_1(\tau^2 a y_1 + \tau b y_2)}{1 - \frac{3}{4}m \cos^2 x_1}. \end{aligned} \tag{6}$$

and the parameter set $\lambda = (a, b, \tau, m)$ is in $\mathbb{R}^4$. System (5)–(6) establishes a nonlinear evolution equation in $C([-1, 0]; \mathbb{R}^2)$, the space of continuous functions on the interval $[-1, 0]$.

Note that, because f is odd, that is,

$$f(-x, -y, \lambda) = -f(x, y, \lambda), \tag{7}$$

the system has the symmetry of reflection in the origin. Consequently, the origin 0 is always an equilibrium, and any solution of (5)–(6) is either symmetric under this symmetry or it is nonsymmetric and its image under reflection in the origin is also a solution.

The linear stability analysis of the origin 0 depending on the parameters a, b, τ, and m shows that there is a bounded region of stability of 0 in the (a, b)-plane if $\tau \in (0, \tau_*)$ where

$$\tau_* = \frac{1}{2}\sqrt{8 - 6m}$$

is the maximal permissible delay for linear stability (this corresponds to a delay time $\sqrt{L(4 - 3m)}/\sqrt{3g}$ in the unscaled time in the original physical quantities); see also Refs. [2,9]. For $\tau \to \tau_*$ the region of linear stability shrinks to the point $a = 1$, $b = \tau_*$ and the origin 0 has a triple-zero eigenvalue singularity. At this point $\lambda_* = (1, \tau_*, \tau_*)$ the linearization of the origin

$$\dot{x}(t) = \begin{pmatrix} 0 & 1 \\ 2 & 0 \end{pmatrix} x(t) + \begin{pmatrix} 0 & 0 \\ -2 & -2 \end{pmatrix} x(t - 1) \tag{8}$$

has an eigenvalue 0 with algebraic multiplicity three and geometric multiplicity one.

Equation (8) is a linear evolution equation in $C([-1, 0]; \mathbb{R}^2)$. It induces an invariant splitting of $C([-1, 0]; \mathbb{R}^2)$ into a direct sum $\mathcal{N} \oplus \mathcal{H}$ where $\mathcal{N}$ is the three-dimensional generalized nullspace of the right-hand-side of (8) and $\mathcal{H}$ is the invariant complement of $\mathcal{N}$ in $C([-1, 0]; \mathbb{R}^2)$. The nonlinear system (5)–(6) is a small perturbation of (8) near the origin for λ near λ_*.

Local center manifold theory for DDEs [7,8] states that there exists a smooth map $H : \mathcal{N} \times \mathbb{R}^4 \to \mathcal{H}$ such that the manifold $\{x_N + H(x_N, \lambda) \in C([-1, 0]; \mathbb{R}^2) : x_N \in \mathcal{N}\}$ is invariant under the evolution of the nonlinear system (5)–(6)

locally around the origin for λ near λ_*. This manifold is called the local center manifold, and the dynamics on it are governed by a three-dimensional ODE. The goal of the center manifold reduction is to find a suitable approximation of this ODE.

Specifically, we expand $\mathcal{N}$ in the basis

$$b_1 = \begin{pmatrix} 1 \\ 0 \end{pmatrix}, \qquad b_2 = \begin{pmatrix} s \\ 1 \end{pmatrix}, \qquad b_3 = \begin{pmatrix} 1 + \frac{1}{2}s^2 \\ s \end{pmatrix} \tag{9}$$

where $s \in [-1, 0]$ acts as the spatial variable in $C([-1, 0]; \mathbb{R}^2)$. The next step is to introduce a small scaling parameter r and zoom into the neighborhood of the origin in phase space and λ_* in parameter space by the change of variables, parameters and time scale:

$$\begin{aligned} x &= r^3 u_1 b_1 + r^5 u_2 b_2 + r^7 u_3 b_3 + r^3 z, \\ (a, b, \tau) &= \left(1 + \alpha \frac{1}{3} r^6,\ \tau_* + \beta \frac{\tau_*}{3} r^2,\ b + \gamma \frac{\tau_*}{3} r^4\right), \\ t_{\text{old}} &= r^2 t_{\text{new}}. \end{aligned} \tag{10}$$

Here $u = (u_1, u_2, u_3) \in \mathbb{R}^3$ is the new magnified variable representing the component of x in the center subspace $\mathcal{N}$, z is the magnified component of x in $\mathcal{H}$, and $\mu = (\alpha, \beta, \gamma) \in \mathbb{R}^3$ is an unfolding parameter of the triple-zero singularity. The three-dimensional local center manifold can be expressed as a graph $z = z(u, \mu, r)$. By using the invariant projections induced by the basis (9), we split system (5)–(6) into an ODE on $\mathcal{N}$ and an evolution equation on $\mathcal{H}$. Then we use the substitution (10) and expand with respect to r; details of these computations can be found in Ref. [13]. The result is that the graph $z(u, \mu, r)$ is of order r^6 and that u satisfies the three-dimensional ODE

$$\begin{pmatrix} \dot{u}_1 \\ \dot{u}_2 \\ \dot{u}_3 \end{pmatrix} = \begin{pmatrix} u_2 \\ u_3 \\ -\alpha u_1 + \gamma u_2 + \beta u_3 + u_1^3 \end{pmatrix} + r^2 R(u, \mu, r) \tag{11}$$

where R is a smooth function of its arguments. Note that affine and quadratic terms are not present in (11) due to the symmetry (7). The form of the linear and the dominant cubic term are determined by the triple-zero singularity. The original parameters (a, b, τ) can be recovered from the unfolding parameter $\mu = (\alpha, \beta, \gamma)$ using (10), and the coefficient in front of the cubic term is independent of the fourth parameter m (and, hence, was scaled to 1).

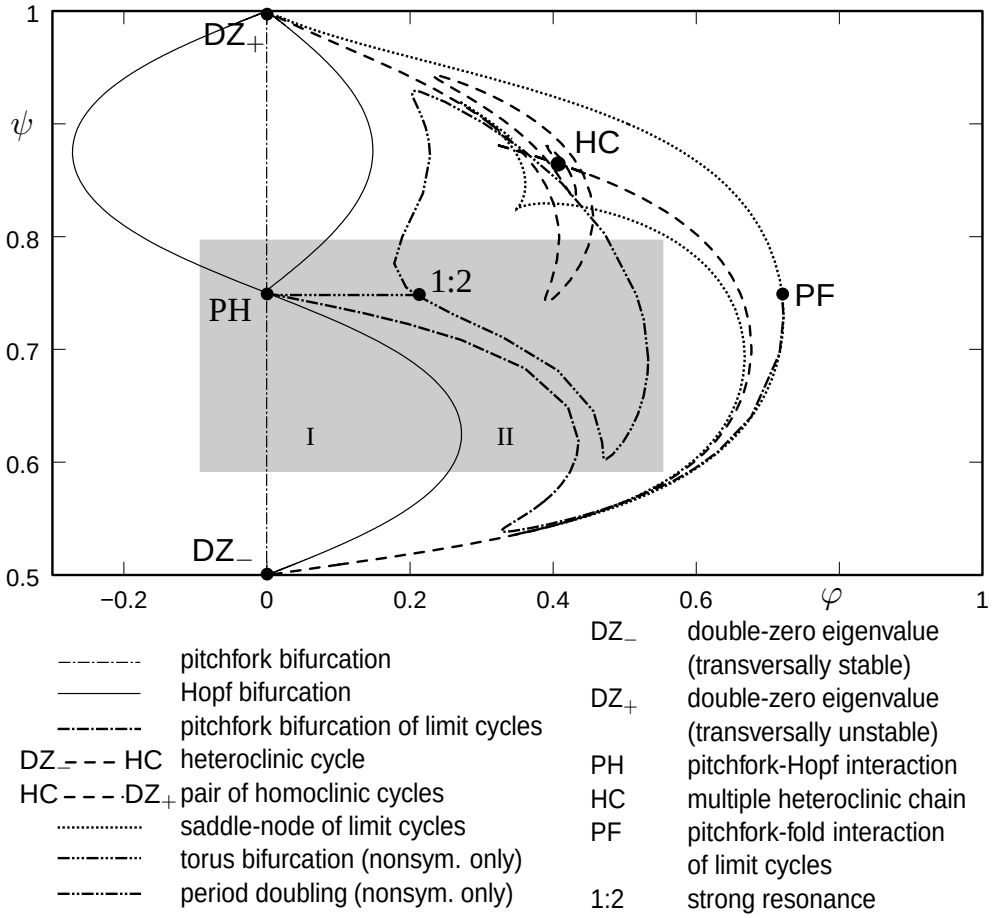

Fig. 2. Bifurcation diagram of the truncated system, system (11) for $r = 0$. The shaded area of the diagram is shown in more detail in Fig. 5.

2.2 Basic dynamics of the reduced system

Consider the truncated system, equation (11) with $r = 0$. Any hyperbolic equilibrium, periodic orbit, or normally hyperbolic invariant manifold in the truncated system persists under the small perturbation by $r^2 R$, and, hence, exists in the full DDE system (5)–(6) for sufficiently small r and for the parameters obtained by (10).

Figure 2 summarizes the results (first obtained in Ref. [13]) of the bifurcation analysis of the reduced system (11) with linear stability analysis in combination with numerical continuation of periodic orbits using AUTO [19]. As the truncated system (11) has cone structure one can restrict the continuation to the parameter sphere $\alpha^2 + \beta^2 + \gamma^2 = 1$, which we parametrize by φ and ψ given by

$$\alpha = \sin\frac{\pi}{2}\varphi, \qquad \beta = \cos\frac{\pi}{2}\varphi\ \cos 2\pi\psi, \qquad \gamma = \cos\frac{\pi}{2}\varphi\ \sin 2\pi\psi. \tag{12}$$

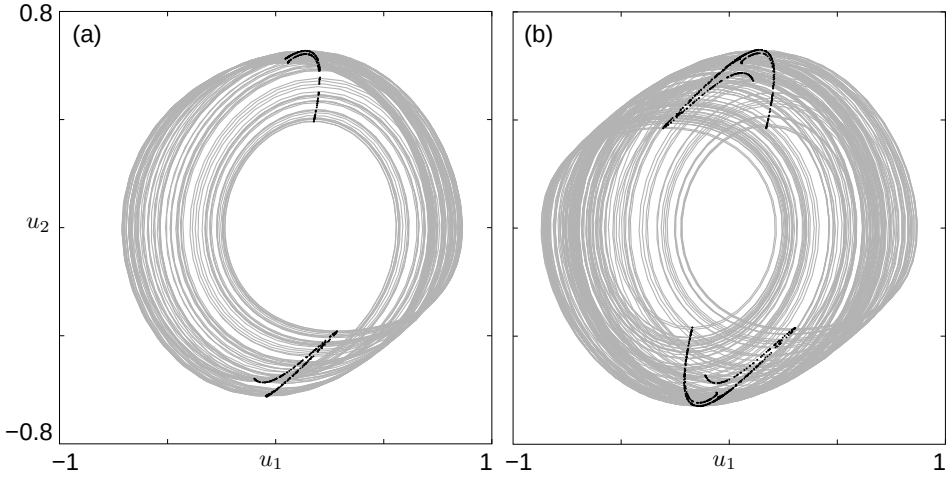

Fig. 3. One of the two coexisting nonsymmetric attractors for $(\varphi, \psi) = (0.4, 0.6958)$ (a) and the symmetric attractor for $(\varphi, \psi) = (0.4, 0.6966)$ (b) as observed in a simulation of the truncated system, (11) with $r = 0$. The intersections of the gray trajectories with the plane $\{u_3 = 0\}$ are shown as black dots.

The region marked by I in Fig. 2 is the region of linear stability of 0. In the region marked by II there is a family of stable symmetric periodic orbits bifurcating from the Hopf bifurcation at 0. These periodic oscillations around the upside-down position were found in experiments in Ref. [11]. Indeed, there is only one two-parameter family of symmetric periodic orbits that is connected to the origin. It exists in a bounded region of the (φ, ψ)-plane. Its left boundary is the symmetric Hopf bifurcation of 0, the S-shaped solid curve connecting the points DZ_-, PH and DZ_+ in Fig. 2. (Note that there is also a Hopf curve of the nonsymmetric saddles between PH and DZ_+.) The right boundary is formed by global bifurcations in which the symmetric periodic orbit disappears, namely the dashed curves in Fig. 2. Along the dashed curve between DZ_- and HC there is a heteroclinic connection between the pair of nonsymmetric saddles. Along the dashed curve connecting DZ_+ and HC a homoclinic figure-eight shaped connection to 0 exists. Throughout the entire region of their existence, the symmetric periodic orbits undergo only saddle-node bifurcations and pitchfork bifurcations, where they lose their stability to a branch of nonsymmetric periodic orbits. Consequently, this primary family of symmetric periodic orbits is the only non-trivial symmetric balancing regime that is 'connected' to the origin in the parameter plane, meaning that it can be found by continuation from 0.

3 Complex symmetric motion in the reduced system

The coexisting stable pair of nonsymmetric periodic orbits that branches from the primary symmetric periodic orbit at the pitchfork bifurcation (the dot-

dashed boundary of region II in Figure 2) undergoes a period doubling bifurcation along the dot-dot-dashed closed curve. This is the first in an infinite sequence of period doublings leading to a pair of nonsymmetric chaotic attractors. Figure 3 shows two attractors in projection onto the (u_1, u_2)-plane for nearby parameter values inside the period doubling island of Fig. 2, obtained by simulations of the truncated system, (11) for $r = 0$. While Fig. 3 (a) shows one of the two nonsymmetric chaotic attractors, Fig. 3 (b) shows a bigger symmetric chaotic attractor. It is created in a crisis bifurcation [20] that 'merges' the two nonsymmetric attractors. Roughly speaking, the attractor in panel (b) can be obtained by overlaying that in panel (a) with its symmetric counterpart, obtained by rotating panel (a) by π. Also shown in Fig. 3 are the intersection points (in black) of the attractors with the plane $\{u_3 = 0\}$; providing evidence that the attractors are indeed chaotic. Each attractor intersects this plane in two locations, one for positive and one for negative u_2. The symmetric attractor in this section in Fig. 3 (b) consists approximately of the two nonsymmetric pieces of the nonsymmetric attractor in Fig. 3 (a).

3.1 Homoclinic tangency

We now give a more precise statement about this mechanism in terms of a homoclinic bifurcation of the Poincaré map to a section, which we choose to be $\{u_3 = 0\}$. This will also allow us to show that stable symmetric periodic orbits exist near symmetric chaotic attractors in so-called periodic windows. These complex symmetric periodic orbits correspond to balancing motion of the pendulum.

As was shown in Fig. 3 the attractors intersect the section $\{u_3 = 0\}$ transversally and in two distinct regions. We define by Π the return map of the flow of the truncated system (11) from each of these regions back to the same region. In other words, the map Π is defined as the second return to the section. The primary symmetric periodic orbit intersects the section in two points transversally along the curve of pitchfork bifurcations shown in Fig. 2. Hence, Π is a Poincaré map for the primary symmetric periodic orbit, a well defined two-dimensional diffeomorphism in its domain of definition, the two regions as defined above. (Note that Π cannot be extended to a global Poincaré map on the entire plane $\{u_3 = 0\}$.) Because the section $\{u_3 = 0\}$ was chosen to contain the origin, the map Π inherits the odd symmetry (7) from the flow. Consequently, we can concentrate on Π in one of the two regions, say, on that for negative u_2. In this region there is a unique fixed point S corresponding to the primary symmetric periodic orbit. After the pitchfork bifurcation (to the right of the dot-dashed curve in Fig. 2) S is a saddle with eigenvalues Λ_1 and Λ_2 satisfying $0 < \Lambda_2 < \Lambda_1\Lambda_2 < 1 < \Lambda_1$. Hence, it has one-dimensional stable and unstable invariant manifolds, $W^s(S)$ and $W^u(S)$, respectively.

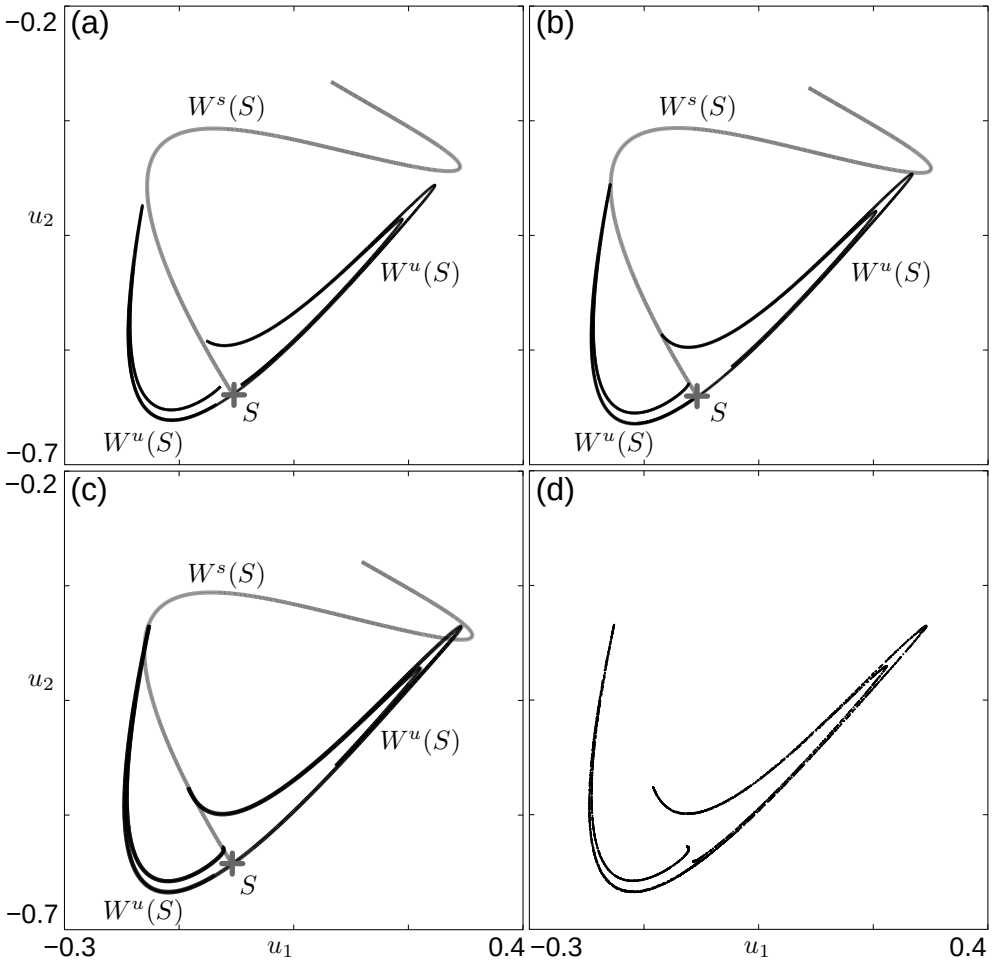

Fig. 4. Unstable and stable manifolds of S for the map Π at the parameter values $\varphi = 0.4$, (a) $\psi = 0.6950$, (b) $\psi = 0.6958$, and (c) $\psi = 0.6966$. Panel (d) shows the result of a long term simulation of Π for $\psi = 0.6966$, corresponding to the arrangement of the invariant manifolds in panel (c).

To show that these manifolds undergo a first quadratic homoclinic tangency we compute appropriate finite parts of these manifolds with a prescribed accuracy. We use the algorithm from Refs. [14,21] in the form of an extension module [22] that works as part of the Tcl/Tk version of the package DsTool [23]. The return map Π is computed by integration of the vector field with a Runge-Kutta fourth order discretization.

Figure 4 shows conclusive evidence that there is indeed a first quadratic tangency, which is crossed with positive velocity under variation of the parameter ψ. Panels (a) to (c) show the fixed point S, one side of its stable manifold $W^s(S)$ and both sides of its unstable manifold $W^u(S)$ for fixed $\varphi = 0.4$ and three different, but close values of ψ. Clearly, $W^s(S)$ and $W^u(S)$ do not intersect in panel (a), but do intersect in panel (c). Because finite initial pieces of these manifolds depend smoothly on parameters, these numerical results provide accurate evidence that a first tangency exists and where it is located.

Panel (b) shows the approximate moment of tangency. Figure 4 (d) is the result of a long-time simulation of Π (after discarding transients) showing an attractor resembling the closure of both parts of $W^u(S)$ for the same parameter values as Fig. 4 (c). This attractor indeed has the properties predicted by theory, which is numerical evidence that it is chaotic.

The importance of the first tangency is that it corresponds to an attractor crisis that creates a single symmetric chaotic attractor of Π by merging two smaller nonsymmetric chaotic attractors that are the result of the period doubling sequence. Before the tangency there are two distinct chaotic attractors of Π, one on each side of the shown branch of $W^s(S)$, consisting of the closure of the respective branch of $W^u(S)$. However, after the tangency it is possible to pass from one side of $W^s(S)$ to the other. This mechanism creates a single attractor and is often referred to as a crisis bifurcation [20]. More specifically, this is a symmetry-restoring (interior) crisis in which two symmetrically related attractors hit the boundary of their basin of attraction simultaneously and merge. It occurs if $W^u(S)$ and $W^s(S)$ have a homoclinic tangency and the union of the nonsymmetric attractors is equal to the closure of the whole unstable manifold $W^u(S)$ at the moment of tangency. This phenomenon was classified as intermittent switching in Ref. [16]. It was observed for example in Ref. [24] in a DDE model (also with $\mathbb{Z}_2$-symmetry) of a laser with phase-conjugate feedback.

The dynamics on the symmetric chaotic attractor follow one of the two nonsymmetric subparts for a long time before crossing $W^u(S)$ to then follow the other part, before switching back, and so on. This corresponds to the inverted pendulum making small chaotic oscillations while leaning to one side at a time. The pendulum does not fall over because the controller compensates by increasing the velocity of the cart, then changing direction and so on. In other words, the velocity of the cart also performs a chaotic motion but with potentially very large excursions depending on the exact nature of the chaotic attractor.

3.2 Existence of symmetric periodic orbits

To make rigorous statements about the existence of complicated symmetric periodic orbits of Π in the vicinity of the homoclinic tangency we perform a symmetry reduction for Π as follows. Let us denote by $\widehat{\Pi}$ the first return to the section composed with the symmetry operation of rotation by π. Then $\widehat{\Pi}$ is a diffeomorphism in the same domain of definition as Π, but it does not have reflectional symmetry in the origin. In particular, the map $\widehat{\Pi}$ satisfies

$$\left(\widehat{\Pi}\right)^2 = \widehat{\Pi} \circ \widehat{\Pi} = \Pi.$$

This means that symmetric periodic orbits of Π correspond to periodic orbits of $\widehat{\Pi}$ with odd period. Similarly, nonsymmetric periodic orbits of Π are periodic orbits of even minimal period of $\widehat{\Pi}$.

In particular, S is a fixed point, that is, a point of (odd) period 1 of $\widehat{\Pi}$. The pitchfork bifurcation of S for Π corresponds to a period doubling bifurcation of S for $\widehat{\Pi}$. After this period doubling, S is a saddle fixed point of $\widehat{\Pi}$. The one-dimensional stable and unstable invariant manifolds of S with respect to $\widehat{\Pi}$ and Π are identical. Thus, we denote them by $W^u(S)$ and $W^s(S)$ for $\widehat{\Pi}$ as well.

The existence of the quadratic tangency of $W^u(S)$ and $W^s(S)$ allows us to apply the well-established theory of homoclinic tangencies in two-dimensional diffeomorphisms; see, for example, Ref. [15]. The saddle value of S for the parameter values of Fig. 4(c) is less than 1, that is, the eigenvalues Λ_j $(j = 1, 2)$ of $\widehat{\Pi}$ at S satisfy the relation

$$\Lambda_1 < -1 < \Lambda_1\Lambda_2 < 0 < \Lambda_2 < 1. \tag{13}$$

The following lemma is an immediate consequence of the general theoretical results [15] for two-dimensional diffeomorphisms close to homoclinic tangencies for saddle fixed points satisfying relation (13).

Lemma 1 *Close to the homoclinic tangency there exist infinitely many open sets of parameters ψ where the map $\widehat{\Pi}$ has stable periodic orbits with odd period.*

Indeed, the general results are much deeper stating that there exist infinitely many stable periodic orbits simultaneously for residual sets in the so called Newhouse regions of the parameter space. We remark that [15] assumes that the map is orientation preserving, which $\widehat{\Pi}$ is not. However, this assumption is not actually necessary for the construction of the stable periodic orbits.

Although these periodic orbits typically have a large period and a small basin of attraction, they are robust with respect to small perturbations of the map. Hence, they exist as symmetric periodic orbits in the non-truncated system (11) and in the full DDE system (5)–(6) as well. Any of these periodic orbits corresponds to a symmetric small-amplitude regime in (5)–(6) with a periodic and, hence, bounded velocity of the cart. In other words, we have found many balancing motions of the inverted pendulum that are given by these more complex symmetric periodic orbits.

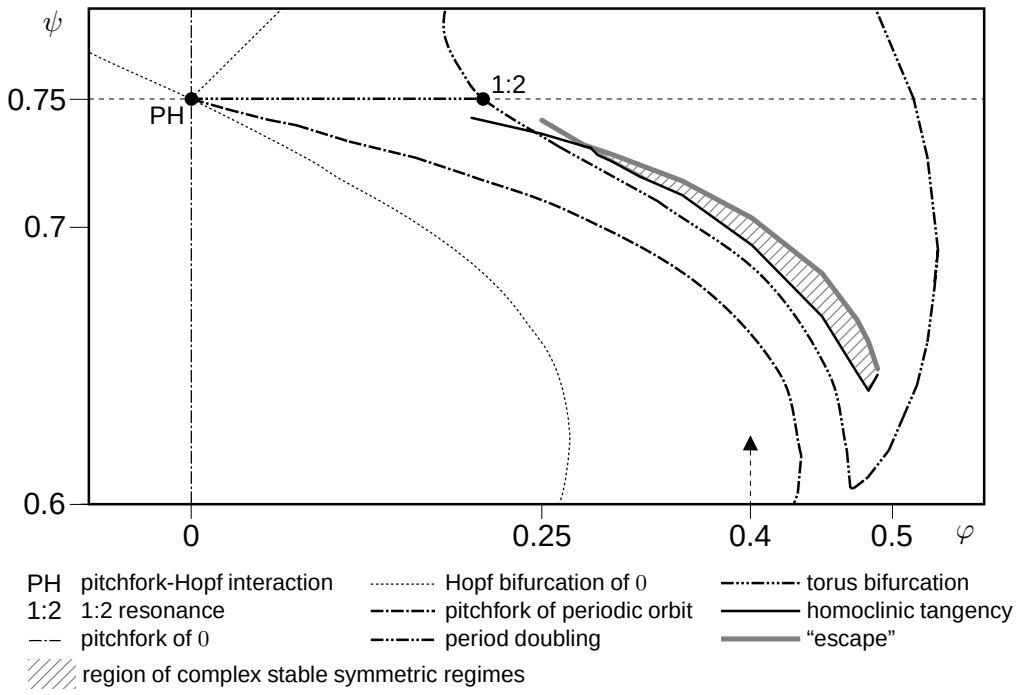

Fig. 5. Curve of homoclinic tangency and the region of stable symmetric attractors in the bifurcation diagram. The arrow shows the line along which we chose the parameter values for Figs. 3, 4 and 6.

3.3 The relevant region in parameter space

The homoclinic tangency of Π (and $\widehat{\Pi}$) to S forms a smooth curve in the (φ, ψ)-plane that is robust with respect to small perturbations, for example, small nonzero r in (11) or numerical errors. In Figure 5 we have added as a solid black polygon an approximation of the curve of homoclinic tangency to S to the bifurcation diagram. The corners of this polygon have been found by identifying the first homoclinic tangency up to 4 digits in φ and ψ. Since the saddle value of S is smaller than 1 along the whole curve, Lemma 1 implies that there exist many regions near the curve of homoclinic tangency where symmetric stable periodic orbits exist.

If the nonsymmetric attractors of Π are equal to the closure of the whole unstable manifold $W^u(S)$ at the curve of homoclinic tangency, one observes an attractor crisis [20] as depicted in Fig. 3 and Fig. 4(d). This defines one boundary of the region in the (φ, ψ)-plane where chaotic symmetric attractors may occur. A numerical approximation of this region is hatched in Fig. 5. Its other boundary is defined by the occurrence of a pair of (symmetrically related) heteroclinic tangencies between S and the pair of nonsymmetric saddle equilibria $E_\pm = (\pm\sqrt{\sin(\pi\varphi/2)}, 0, 0)$ of the truncated system (11). The saddles $E_\pm$ both have a two-dimensional stable manifold $W^s(E_\pm)$. The intersections

of these stable manifolds with the plane $\{u_3 = 0\}$ generically are curves that establish the boundary between the existence of stable bounded dynamics of Π and escape to infinity. Consequently, a tangency between $W^u(S)$ and $W^s(E_+)$ (and simultaneously between $W^u(S)$ and $W^s(E_-)$) is a codimension-one bifurcation that defines the boundary of the parameter region where Π can have stable bounded regimes. The heteroclinic tangency forms a smooth curve in the (φ, ψ)-plane, which we approximated by the thick gray polygon in Figure 5. The corners were found by checking the boundedness of a numerical trajectory over large integration times. We started simulations in the vicinity of the nonsymmetric fixed points of Π and checked whether the orbit escapes to infinity within 15000 iterates of Π. (Note that the return map Π is not well defined near the saddles $E_\pm$, such that algorithms for computing one-dimensional manifolds cannot be readily applied.)

We remark that, at the moment of the homoclinic tangency, the (chaotic) nonsymmetric attractors may be substantially smaller than the closure of the unstable manifold $W^u(S)$. In this case, there is no attractor crisis at the tangency, but a change in the basin of attraction of the nonsymmetric attractor (also referred to as a basin boundary metamorphosis [20]). This happens along the part of the black solid tangency curve in Fig. 5 that does not bound the shaded region, to the left of the codimension-two point where the black and gray curves meet. (This point appears to be what is known as a double crisis vertex [25] in systems without symmetry.) In fact, the tangency curve even crosses the period doubling curve (for $\varphi < 0.25$), so that the homoclinic tangency takes place when the two nonsymmetric fixed points of Π are stable.

4 Complex symmetric motion in the full DDE system

The center manifold reduction (see Section 2) guarantees that all phenomena observed in the truncated system (11) that are robust with respect to small perturbations are also present in the full DDE system (5)–(6). In particular the curves of period doubling, and homoclinic and heteroclinic tangency shown in Fig. 5 will persist. This implies the existence of symmetric high-period periodic attractors and of symmetric chaotic attractors in the hatched region of Fig. 5 for the DDE system as well.

Furthermore, in Ref. [13] we could establish a very good quantitative agreement between the bifurcation diagrams of the truncated system and that of the full DDE system even quite far away from the triple-zero singularity. However, symmetric chaotic attractors of Π may not be robust in the sense of persistence with respect to small perturbations, and the complex stable symmetric periodic orbits, while being robust according to Lemma 1, may have extremely small basins of attraction and are typically difficult to find. Hence, it is worth

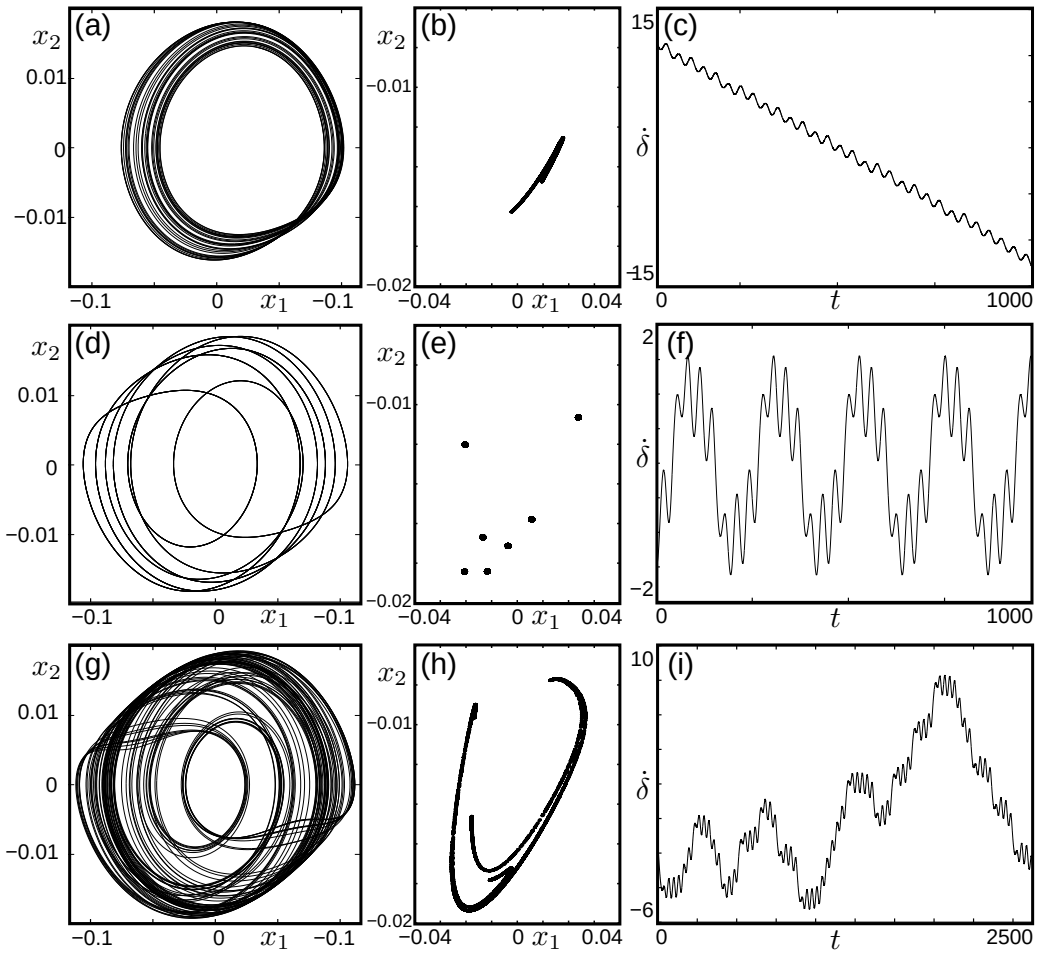

Fig. 6. Simulation results for DDE system (5)–(6),(14) with $m = 0$ demonstrating the transition to symmetric attractors. The first column shows the projection onto the (x_1, x_2)-plane, the second column shows the projection of a Poincaré map, the third column shows the time trace of the velocity of the cart $\dot{\delta}$. Parameter values are $\varphi = 0.4$ and $\psi = 0.702$ for (a)–(c), $\psi = 0.705$ for (d)–(f), and $\psi = 0.71$ for (g)-(i).

illustrating numerically that we can observe the phenomena described in section 3 in the full DDE system (5)–(6) as well. We set the scaling parameter to $r = 0.5$ and the mass ratio to $m = 0$. (Note that m only enters in the formula for τ^*.) To convert the parameters φ and ψ back to the original parameters a, b, and τ we use the scaling (10) and transformation (12). The velocity of the cart is governed by the equation

$$\ddot{\delta}(t) = L\frac{\frac{m}{2}x_1(t)x_2(t)^2 + \frac{2}{3}[a\tau^2 x_1(t-1) + b\tau x_2(t-1)] - \frac{m}{4}\tau^2\sin(2x_1(t))}{1 - \frac{3m}{4}\cos^2 x_1(t)} \quad (14)$$

in the time scale corresponding to a delay of 1. We simulate the full DDE system (5)–(6), (14) for x and $\dot{\delta}$ using a 4th-order fixed step Adams-Bashforth method with a stepsize of 0.05.

Figure 6 shows simulation results for three different parameter values near $(\varphi, \psi) = (0.4, 0.7)$, after discarding a transient of duration 5000. Three different regimes are shown by three panels each. The first panel shows the $(x_1(t), x_2(t))$-projection of the attractor of the DDE. The second panel shows the attractor of the Poincaré map defined by the second return to the hyperplane $\{x_2(t) - x_2(t - 0.05) = 0\}$ (by only plotting the head point). The third panel shows the corresponding time profile of the cart velocity $\dot{\delta}(t)$. Panels (a) and (b) show a nonsymmetric chaotic attractor, which does not correspond to successful balancing, since $|\dot{\delta}(t)|$ increases on average according to panel (c). Panel (d) and (e) show a symmetric periodic orbit. It corresponds to successful balancing motion because $\dot{\delta}(t)$ remains bounded as can be seen from panel (f). Finally, panels (g) and (h) show a symmetric chaotic attractor and panel (i) the corresponding motion of the cart velocity. The dynamics of the cart velocity in panel (i) consists of large irregular excursions with a zero mean. Therefore, seen over a sufficiently long timescale, the velocity of the cart resembles a random walk.

We remark that it was checked with extended simulations that the attractors in Fig. 6(a), (b), (g) and (h) are indeed examples of chaotic attractors (which must exist according to theory). The computed trajectories do not repeat over an integration time of 1.5×10^5. Note that panels (a) and (g) only show a short segment of the computed trajectory so that the structure of the respective attractor is visible, while the panels (b) and (h) show the entire computed attractor of the Poincaré map.

In summary, Fig. 6 shows that the symmetric attractors that exist in the reduced system according to Lemma 1 can indeed be found in numerical simulations of the full DDE. In particular, complex balancing motion due to complicated symmetric periodic orbits exists even quite far away from the triple-zero singularity.

5 Discussion and conclusions

The controlled inverted pendulum is a model case for investigating nonlinear phenomena due to delay-induced instabilities. Previous [1,9,17] and recent [11,13] studies considered the linear stability of the origin and found a primary family of small-scale (symmetric) periodic balancing motions branching off in a Hopf bifurcation. We showed that more complex balancing motions are possible. The mechanism that gives rise to this behavior is a homoclinic tangency in which two nonsymmetric attractors collide and form a bigger symmetric attractor.

While existing models for small chaotic oscillations require nonlinearities (such

as round-off) of the control loop, our results show that complex balancing motions are possible and supported in a system with a linear PD controller, where the geometric nonlinearity of the controlled mechanical system is the only (weak) nonlinearity. The mechanism we found occurs naturally in a neighborhood of the symmetric triple-zero singularity. Therefore, one must expect the emergence of complex symmetric attractors in many other systems — in particular, in other symmetric control problems with delay.

A characteristic feature of the complex balancing motions described in this paper is that they are located in islands in the parameter space that are isolated from the stability regions of the origin and the primary periodic orbits. While some of these islands may be big enough to be accessible experimentally, they will be difficult to find experimentally (it was already difficult to find them in the model) because they cannot simply be reached by following a known solution under variation of a parameter. Finding complex balancing regimes in an experiment is a challenging open problem.

A related open question is whether the more complex phenomena described in this paper can also be found in more realistic balancing models. For example, the model compared with the experiments in Ref. [11] included viscous friction and a component of the control force D depending on the displacement δ and the velocity $\dot{\delta}$ of the cart (in order to keep δ near 0). This is an interesting and challenging question because even small friction and a weak dependence of D on δ and $\dot{\delta}$ are singular perturbations of (2)–(3).

Acknowledgments

The research of J.S. is supported by EPSRC grant GR/R72020/01 and that of B.K. by an EPSRC Advanced Research Fellowship.

References

[1] J. L. Cabrera, J. G. Milton, On-off intermittency in a human balancing task, Physical Review Letters 89 (158702).

[2] G. Stépán, L. Kollár, Balancing with reflex delay, Mathematical and Computer Modelling 31 (2000) 199–205.

[3] C. M. Marcus, R. M. Westervelt, Stability of analog networks with delay, Phys. Rev. A 39 (1989) 347–359.

[4] L. P. Shayer, S. A. Campbell, Stability, bifurcation, and multistability in a system of two coupled neurons with multiple time delays, SIAM J. of Appl. Math. 61 (2) (2000) 673–700.

[5] B. Krauskopf, D. Lenstra (Eds.), Fundamental Issues of Nonlinear Laser Dynamics, American Institute of Physics, 2000.

[6] F. C. Moon, Dynamics and Chaos in Manufacturing Processes, Wiley, New York, 1998.

[7] J. K. Hale, S. M. V. Lunel, Introduction to Functional Differential Equations, Vol. 99 of Applied Mathematical Sciences, Springer-Verlag, 1993.

[8] O. Diekmann, S. van Gils, S. M. V. Lunel, H.-O. Walther, Delay Equations, Vol. 110 of Applied Mathematical Sciences, Springer-Verlag, 1995.

[9] G. Stépán, Retarded Dynamical Systems: Stability and Characteristic Functions, Longman Scientific and Technical, 1989.

[10] S. A. Campbell, J. Bélair, Analytical and symbolically-assisted investigation of Hopf bifurcation in delay-differential equations, Canadian Applied Mathematics Quarterly 3 (2) (1995) 137–154.

[11] M. Landry, S. A. Campbell, K. Morris, C. Aguilar, Dynamics of an inverted pendulum with delayed feedback control, Preprint, University of Waterloo, submitted (2003).

[12] G. Haller, G. Stépán, Micro-chaos in digital control, J. Nonlinear Sci. 6 (1996) 415–448.

[13] J. Sieber, B. Krauskopf, Bifurcation analysis of an inverted pendulum with delayed feedback control near a triple-zero eigenvalue, Nonlinearity 17 (1) (2004) 85–104.

[14] B. Krauskopf, H. M. Osinga, Growing 1D and quasi 2D unstable manifolds of maps, J. Comp. Phys. 146 (1) (1998) 404–419.

[15] J. Palis, F. Takens, Hyperbolicity and sensitive chaotic dynamics at homoclinic bifurcations, Cambridge studies in advanced mathematics, Cambridge University Press, 1993.

[16] C. Grebogi, E. Ott, F. Romeiras, J. Yorke, Critical exponents for crisis-induced intermittency, Phys. Rev. A 36 (11) (1987) 5365–5380.

[17] F. M. Atay, Balancing the inverted pendulum using position feedback, Appl. Math. Letters 12 (1999) 51–56.

[18] J. Sieber, B. Krauskopf, Extending the permissible control loop latency for the controlled inverted pendulum, Applied Nonlinear Mathematics Research Report 2004.13, University of Bristol
(`http://www.enm.bris.ac.uk/anm/preprints/2004r13.html`).

[19] E. J. Doedel, A. R. Champneys, T. F. Fairgrieve, Y. A. Kuznetsov, B. Sandstede, X. Wang, AUTO97, Continuation and bifurcation software for ordinary differential equations (1998).

[20] K. Alligood, T. Sauer, J.A. Yorke, Chaos: An Introduction to Dynamical Systems, Springer, New York, 1997.

[21] B. Krauskopf, H. M. Osinga, Investigating torus bifurcations in the forced Van der Pol oscillator, in: E. Doedel, L. Tuckerman (Eds.), Numerical Methods for Bifurcation Problems and Large-Scale Dynamical Systems, Vol. 119 of IMA Vol. Math. Appl., Springer-Verlag, 2000.

[22] J. England, B. Krauskopf, H. Osinga, Computing one-dimensional stable manifolds of planar maps without the inverse, Preprint 2003.02, University of Bristol, Bristol Centre for Applied Nonlinear Mathematics (2003).

[23] A. Back, J. Guckenheimer, M. Myers, F. Wicklin, P. Worfolk, DsTool: computer assisted exploration of dynamical systems, Notices Amer. Math. Soc. 39 (4) (1992) 303–309.

[24] B. Krauskopf, G.R. Gray, D. Lenstra, Semiconductor laser with phase-conjugete feedback: dynamics and bifurcations, Phys. Rev. E 58 (1998) 7190–7197.

[25] H. B. Stewart, Y. Ueda, C. Grebogi, J. A. Yorke, Double crises in two-parameter dynamical systems, Phys. Rev. Lett. 75 (13) (1995) 2478–2481.